Origin of torsion-induced conductance oscillations in carbon nanotubes

K. S. Nagapriya,[1] Savas Berber,[2,*] Tzahi Cohen-Karni,[1,†] Lior Segev,[1] Onit Srur-Lavi,[1] David Tománek,[2,‡] and Ernesto Joselevich[1,§]

[1]*Department of Materials and Interfaces, Weizmann Institute of Science, Rehovot 76100, Israel*

[2]*Physics and Astronomy Department, Michigan State University, East Lansing, Michigan 48824-2320, USA*

(Received 29 September 2008; published 21 October 2008)

We combine electromechanical measurements with *ab initio* density-functional calculations to settle the controversy about the origin of torsion-induced conductance oscillations in multiwall carbon nanotubes. Contrary to intuition, the observed oscillation period in multiwall tubes exhibits the same inverse-squared diameter dependence as in single-wall tubes with the same diameter. This finding suggests an intrawall origin of the oscillations and an effective electronic decoupling of the walls, which we confirm in calculations of multiwall nanotubes subject to differential torsion. We exclude the alternative origin of the conductance oscillations due to changes in the interwall registry, which would result in a different diameter dependence of the oscillation period.

DOI: 10.1103/PhysRevB.78.165417 PACS number(s): 81.07.De, 73.63.Fg, 85.35.Kt, 85.85.+j

I. INTRODUCTION

The electronic response of carbon nanotubes (CNTs) (Ref. 1) to mechanical deformations is currently a subject of high interest.[2–8] Electromechanical measurements offer fundamental insight into the quantum behavior of electrons in quasi-one-dimensional systems, and also open the way to intriguing applications in nanoelectromechanical systems (NEMS).[9–11] Whereas in single-layer systems, such as single-wall nanotubes (SWNTs) and graphene, conductance depends only on intralayer properties; in systems with multiple layers, such as multiwall nanotubes (MWNTs) and graphite, interlayer coupling brings additional complexity into the picture. Since the typical diameter of MWNTs is larger than that of SWNTs, MWNTs exhibit a higher density of quantized subbands, causing sensitive response to deformations. Studying conductance in nanotubes subjected to torsion is a powerful tool in probing the relative role of intrawall and interwall effects. Previous studies report monotonic changes in the conductance of twisted SWNTs (Ref. 8) in agreement with theoretical predictions,[12] whereas conductance oscillations have been observed in MWNTs under torsion.[7] Discriminating between intrawall and interwall effects as the origin of the observed torsion-induced conductance changes in MWNTs is of fundamental importance for our understanding of the electronic interwall coupling in a MWNT (Refs. 13 and 14) and interlayer coupling in graphene multilayers.

Here we combine diameter-dependent electromechanical measurements with *ab initio* density-functional calculations to settle the controversy of whether observed torsion-induced conductance oscillations in multiwall nanotubes have an intrawall or an interwall origin. For an intrawall origin, the conductance oscillations in a MWNT should be closely related to those in a hypothetical SWNT with the same diameter when subjected to differential torsion. There, the fundamental band gap is periodically modulated as the Fermi momentum $\mathbf{k_F}$ crosses $\mathbf{k}$ subband quantization lines, as seen in Fig. 1(c), while the nanotube is twisted.[7,12,15] Neglecting the effect of interior walls of a MWNT on conductance is justified by our computational results, which indicate that differential torsion effectively decouples the walls on a MWNT near the Fermi level. The alternative interwall origin of the oscillations would be expected if conductance were strongly affected by changes in the interwall registry while the outermost wall of a MWNT is rotated[16] or twisted[17,18] with respect to the inner walls. We find the intrawall effect to dominate in MWNTs, as it predicts the conductance oscillation period to change with the inverse square diameter of the nanotube, in accordance with our measurements, rather than the inverse diameter, as suggested by the latter model.

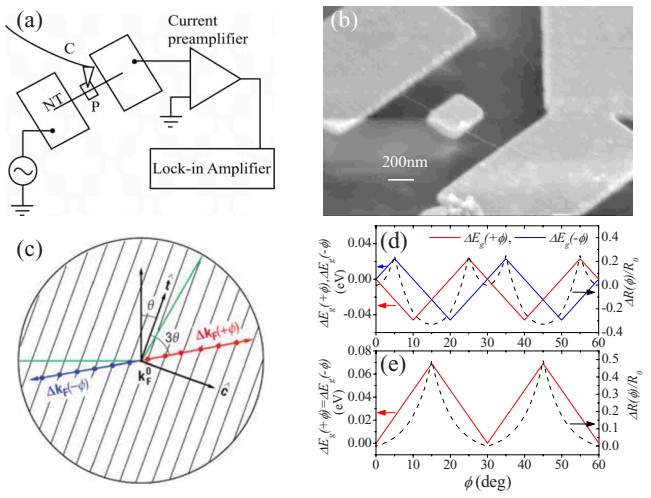

FIG. 1. (Color online) (a) Schematic of the setup. C is the AFM cantilever, NT the nanotube, P the pedal. (b) SEM image of the carbon nanotube-pedal device. (c) Schematic of the shifting of the Fermi momentum $\mathbf{k_F}$ with torsion. The boundary near $\mathbf{k_F}$, located at a corner of the first Brillouin zone of graphene, is indicated by the green lines. Black parallel lines are the allowed $\mathbf{k}$ subbands of the nanotube. The red and blue lines show the shift in $\mathbf{k_F}$ for the left and right segments of the nanotube, respectively. (d), (e) Left axis: Change in the band gap with torsion (solid line) for the two halves of the nanotube. Right axis: The relative resistance change (dashed line) due to the band-gap change for (d) a semiconducting and (e) a metallic nanotube.

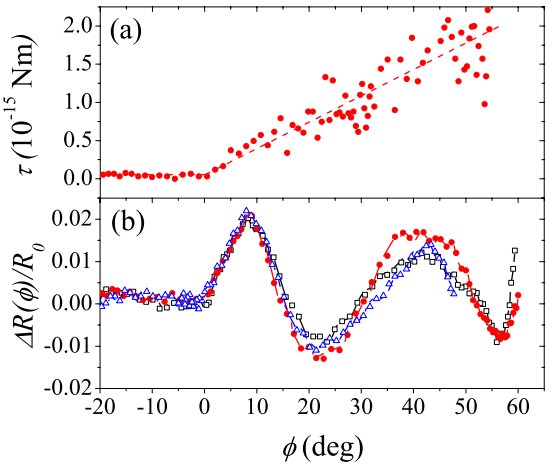

FIG. 2. (Color online) Reproducible conductance oscillations in a 18 nm wide nanotube induced by torsion. (a) Torque and (b) relative resistance change as a function of the torsion angle ϕ.

II. EXPERIMENTAL

A schematic of the experiment is shown in Fig. 1(a). The experimental details are essentially the same as reported in the measurement of torsional electromechanical oscillations in carbon nanotubes.[7] Briefly, MWNTs grown by arc discharge are suspended in 1,2-dichloroethane and spin coated on an oxidized Si substrate. Contact pads and the pedal are fabricated by electron-beam lithography followed by deposition of Cr (5 nm) and Au (90 nm). The pedal is suspended by wet etching followed by critical-point drying using supercritical CO_2. Figure 1(b) shows an SEM image of one such device. The pedal is pressed by an AFM tip (as shown in the schematic) to twist the suspended nanotube. The torque and torsional strain on the nanotube and its conductance are measured simultaneously as the nanotube gets twisted.

III. RESULTS AND DISCUSSION

The torque τ experienced by the nanotube as a function of the torsion angle ϕ is plotted in Fig. 2(a). Nonzero torque indicates that the pedal is being pressed, thereby twisting the nanotube. Figure 2(b) shows the oscillatory behavior in the relative resistance change $\Delta R(\phi)/R_0$ as the nanotube gets twisted, with $R_0=R(\phi=0)$ as the reference. The observed behavior is reproducible for several press-retract cycles.

Figure 3 displays the relative change in resistance $\Delta R(\phi)/R_0$ as a function of ϕ for a few representative MWNT diameters. The gradual increase in the oscillation period $\delta\phi$ with decreasing nanotube diameter is evident. The oscillation period for every MWNT was obtained by taking an average from several press-retract cycles. The dependence of the observed oscillation period $\delta\phi_{\text{obs}}$ on the MWNT diameter d is shown in Fig. 4(a) by squares.

A. Consequences of the intrawall effect

To interpret these results, we first examine the consequences of the intrawall effect, which arises from the shift in $\mathbf{k_F}$, on the nanotube conductance. For a nanotube under torsion, the shift in $\mathbf{k_F}$ relative to the invariant $\mathbf{k}$ lines in the circumferential direction [Fig. 1(c)] is given by $\Delta k_F^c = \phi d \sin(3\theta_0)/(2ld_{\text{C-C}})$.[7,12] Here l is the length of the twisted section of the nanotube and $d_{\text{C-C}}$ is the carbon-carbon bond length. θ_0 is the chiral angle of the untwisted nanotube, defined as the angle between the roll-up vector and the nearest armchair direction in the graphene plane.

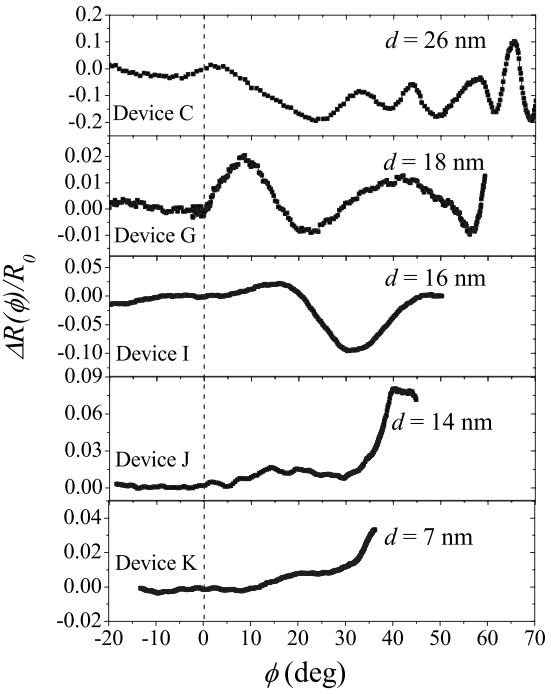

FIG. 3. Relative resistance change as a function of the torsion angle ϕ for nanotubes of different diameter d.

Due to the linearity of the energy dispersion relation near $\mathbf{k_F}$, the band gap E_g is proportional to the distance of $\mathbf{k_F}$ in the circumferential direction from the nearest $\mathbf{k}$ subband. Therefore, ΔE_g initially changes in a linear fashion with torsion. However, when $\mathbf{k_F}$ reaches one of the $\mathbf{k}$ lines, the band gap vanishes and further torsion causes renewed opening of the gap. The band gap reaches its maximum at the midpoint between two $\mathbf{k}$ subbands, where further torsion decreases its value. Thus, the band gap oscillates between zero and its

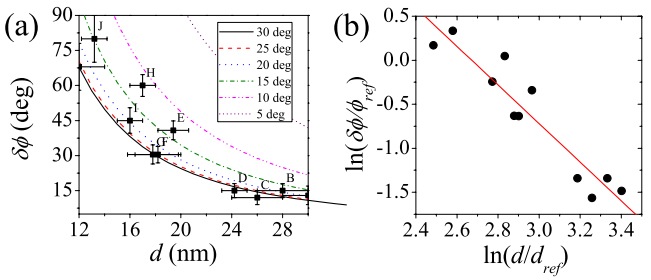

FIG. 4. (Color online) (a) Dependence of the oscillation period $\delta\phi$ on the diameter d. Experimental data $\delta\phi_{\text{obs}}$ are shown by squares. Theoretical predictions for different chiralities, obtained from Eq. (3), are shown by lines. The data points for each nanotube represent averages over several press-retract cycles. (b) $\ln(\delta\phi/\phi_{\text{ref}})$ as a function of $\ln(d/d_{\text{ref}})$, with $\phi_{\text{ref}}=1$ rad and $d_{\text{ref}}=1$ nm. Our data can be fitted by a straight line with a slope of -2.19 ± 0.25.

maximum value, leading to periodic metal-semiconductor transitions (*M-S* effect). Torsion-induced band gap changes are thus given by

$$\Delta E_g = \frac{6\gamma_0 d_{\text{C-C}}}{d}\left[\frac{d^2 \sin(3\theta_0)}{4 d_{\text{C-C}} l}\phi + \Delta j\right], \tag{1}$$

where Δj is an integer corresponding to the change in the quantum number associated with the nearest subband before and after twisting. Simulated ΔE_g for a CNT of $d=18$ nm is plotted in Figs. 1(d) and 1(e). Figure 1(d) shows ΔE_g for an initially semiconducting nanotube. Since the two halves of the CNT experience opposite torsion angles when the pedal is pressed, ΔE_g for each half is shown separately. Figure 1(e) shows ΔE_g for an initially metallic CNT, in which case the change in the band gap is the same for both halves.

The $\Delta R(\phi)/R_0$ resulting from the ΔE_g is given by

$$\frac{\Delta R(\phi)}{R_0} = \frac{1}{A}\left\{\frac{1}{2}\left[e^{\Delta E(\phi)/k_B T + \Delta E(-\phi)/k_B T}\right] - 1\right\},$$

$$A \equiv 1 + \left(\frac{4e^2|t|^2 R_c}{h} + 1\right)e^{-E_0/k_B T}, \tag{2}$$

where $\Delta E(\phi)$ is the torsion-induced change in the activation energy, equal to $\Delta E_g/2$. A is an attenuation factor, R_c is the contact resistance, h is Planck's constant, e is the electron charge, $|t|^2$ is the transmission probability,[7] and E_0 is the initial activation energy. Thus, $\Delta R(\phi)/R_0$ has the same oscillation period as ΔE_g. This can also be seen from Figs. 1(d) and 1(e), where $\Delta R(\phi)/R_0$ is shown by the dashed lines.

For a nanotube of diameter d, the subband spacing is $\delta k = 2/d$. Therefore, the conductance oscillations occur with the period $\Delta k_F^c = 2/d$, which translates to

$$\delta\phi = \frac{4}{d^2}\frac{l d_{\text{C-C}}}{\sin(3\theta_0)}. \tag{3}$$

This master equation for torsion-induced conductance oscillations provides the following insights: (i) The minimum oscillation period for a nanotube of a particular diameter is given by $\delta\phi_{\min} = 4 l d_{\text{C-C}}/d^2$, which is shown by the solid line in Fig. 4(a). The figure clearly indicates that $\delta\phi_{\text{obs}} > \delta\phi_{\min}$ within experimental error. (ii) When a zigzag nanotube with $\theta_0 = 0$ is twisted, $\mathbf{k_F}$ moves parallel to the $\mathbf{k}$ lines, thus keeping the band gap constant. This also follows from Eq. (3), which suggests that $\delta\phi \to \infty$ as $\theta_0 \to 0$. However, assuming a homogeneous distribution of chiralities, we can expect $\approx 83\%$ of the nanotubes to have chiralities in the range of $5° - 30°$ and $\approx 67\%$ to have chiralities between 10° and 30°. Also plotted in Fig. 4(a) by various broken lines is the theoretical value of $\delta\phi$ according to Eq. (3) for chiralities between 5° and 30°. All experimental points lie in the chirality range of $10° - 30°$. We speculate that this could simply be because the chirality distribution may not be homogeneous and higher chiralities are favored during the MWNT growth. Another possible reason is that strain-induced displacements of the triangular sublattices in graphene, known to change the band gap,[19] have been neglected. We thus expect even zigzag nanotubes to change their conductance with torsion. This could mean that our estimated nanotube chiralities may be higher than the actual values. (iii) A plot of $\ln(\delta\phi/\phi_{\text{ref}})$ versus $\ln(d/d_{\text{ref}})$ should give a straight line with the slope −2. A linear fit of the data shown in Fig. 4(b) yields an optimum slope of -2.19 ± 0.25, clearly indicating that the oscillation period $\delta\phi$ is proportional to $1/d^2$, as predicted by Eq. (3).

B. Consequences of the interwall effect

The alternative origin of the conductance oscillations is an interwall effect, examined below. The changes in registry between the walls of a MWNT as the outermost wall is twisted could modify the electronic coupling between the walls, causing changes in conductance. Considering only the outermost and the neighboring inner wall, the double-wall nanotube structure forms a Moiré pattern, which can be thought of as beats in two dimensions. Therefore, for a particular shear strain ξ, the number of coincidences in the Moiré pattern varies linearly with ξ. $\delta\phi$ should then be inversely proportional to the number of these coincidences, $\delta\phi \propto 1/\xi$. Since $\xi \propto d$, we would expect $\delta\phi \propto 1/d$. Our observation of a different functional dependence, $\delta\phi \propto 1/d^2$, thus excludes the Moiré effect as the origin of the conductance oscillations.

C. Theoretical basis for the dominance of the intrawall effect

In order to understand the apparent absence of the Moiré effect and justify neglecting of the interwall interactions when determining the band gap, we performed geometry optimization and electronic structure calculations of corresponding model systems. We used the *ab initio* density-functional theory (DFT) formalism in the local-density approximation (LDA), as implemented in the SIESTA code,[20] with a double-ζ basis set including polarization orbitals, and a mesh cut-off energy of 200 Ry. We used an ultrafine k-point mesh equivalent to a 201×201 k-point sampling of the graphene Brillouin zone, including the Γ point. All structures were optimized until all force components on atoms were less than 0.01 eV/Å. The calculated in-layer bond length $d_{\text{C-C}} = 1.42$ Å and the interlayer spacing $c = 3.34$ Å in the optimized structure of bulk hexagonal graphite showed a deviation of no more than 1% from the experimental data.[21]

Before addressing twist-related changes in the transport of MWNTs, we investigate the effect of interwall interaction on the electronic structure of double-wall nanotubes (DWNTs), which, especially in the limiting case of very large diameters, should closely resemble that of graphene bilayers. Since it is extremely unlikely to find $(n_1,m_1)@(n_2,m_2)$ DWNTs with chiral indices representing a commensurate structure of adjacent walls, corresponding to AA or AB stacked graphene bilayers, we will focus on the general case of incommensurate DWNT structures. The counterpart of a DWNT with incommensurate (n_1,m_1) and (n_2,m_2) walls is a graphene bilayer, where the upper layer has been rigidly rotated–within its plane–with respect to the layer below. Both in DWNTs and graphene bilayers, for specific rotation angles or chiral index combinations, we commonly find quasicommensurate arrangements with large but finite unit cells, associated with Moiré patterns. With the graphene layers in a bi-

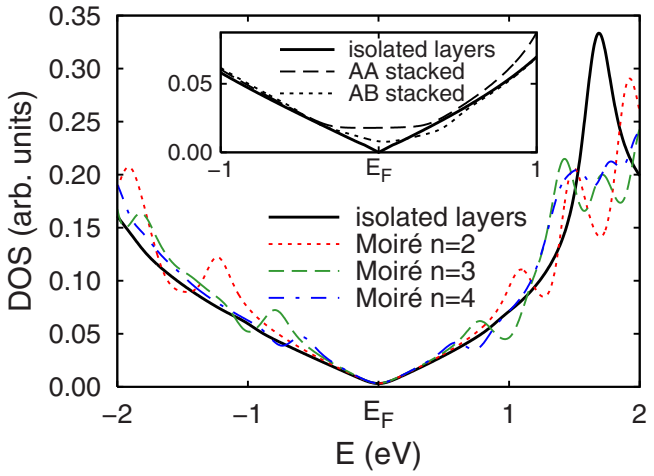

FIG. 5. (Color online) Electronic density of states (DOS) of graphene bilayers. Near the Fermi level, the DOS of isolated layers (solid line) agrees well with that of bilayers forming Moiré patterns with $n=2,3,4$. The DOS of AA and AB stacked bilayers is compared to that of isolated layers in the inset.

layer being spanned by the primitive lattice vectors $\mathbf{a_1}$ and $\mathbf{a_2}$, a Moiré pattern can be produced by rotating the initially coinciding layers about one site so that the lattice point $n\mathbf{a_1}+(n-1)\mathbf{a_1}$ in the upper layer aligns with the lattice point $(n-1)\mathbf{a_1}+n\mathbf{a_1}$ in the lower layer.

In Fig. 5 we compare the density of states (DOS) of a graphene monolayer to that of AA and AB stacked bilayers and bilayers forming Moiré patterns with $n=2,3,4$. Our results show that a graphene monolayer is a zero-gap semiconductor, whereas commensurate AA or AB bilayers are metallic. The cause is the finite interlayer coupling, combined with the favorable symmetry in the latter systems, which introduces new states near E_F. Due to the lack of such symmetry in graphene bilayers forming Moiré patterns, we find no signature of the interlayer coupling in the electronic structure near the Fermi level. As seen in Fig. 5, the electronic density of states of such incommensurate structures is nearly identical to that of isolated graphene monolayers. This finding holds even in presence of the interlayer interaction, which modulates the interlayer separation and coupling by up to 3% due to the presence of Moiré patterns. Using our graphene–nanotube analogy, we conclude that the electronic structure of individual walls in a MWNT is decoupled from that of adjacent walls in the most common case of incommensurability.

Consequently, changes in transport properties of multiwall nanotubes, contacted only at the outermost wall in the present study, can be understood by ignoring the presence of the inner walls, except for their structural support that prevents deformation or collapse of the outermost wall. In particular, the observed conductance changes in twisted MWNTs can be interpreted using the formalism of Yang and Han,[12] developed for an isolated SWNT with the diameter of the MWNT.

IV. CONCLUSIONS

In summary, we identified the origin of conductance oscillations in MWNTs subjected to torsion as a purely intrawall effect, induced by shifting the Fermi momentum across quantization lines, thus periodically opening and closing the fundamental band gap. This striking finding implies an effective electronic decoupling of the walls near the Fermi level, which we confirm in electronic structure calculations of MWNTs subject to differential torsion. Experimental evidence for an intrawall origin is the observed behavior of the conductance oscillation period, which changes with the inverse square diameter of the nanotube. We can exclude the alternative origin of the conductance oscillations due to changes in the interwall registry, as we did not observe proportionality to the inverse nanotube diameter. From this investigation we learned that, from an electromechanical perspective, a MWNT can be regarded as a highly independent set of coaxial SWNTs.

ACKNOWLEDGMENTS

We thank A. Yoffe and S. R. Cohen for assistance with the clean room and AFM, respectively. This research was supported by the Israel Science Foundation, the Kimmel Center for Nanoscale Science, the Israeli Ministry of Defense, Minerva Stiftung, and the Djanogly, Alhadeff, and Perlman foundations. K.S.N. acknowledges the Feinberg Graduate School for support. D.T. and S.B. were supported by the National Science Foundation under NSF-NSEC Grant No. 425826 and NSF-NIRT Grant No. ECS-0506309.

*Permanent address: Physics Department, Gebze Institute of Technology, 41400 Gebze, Kocaeli, Turkey

†Present address: Harvard University, 12 Oxford Street, Cambridge, MA 02138

‡tomanek@pa.msu.edu

§ernesto.joselevich@weizmann.ac.il

[1] A. Jorio, M. Dresselhaus, and G. Dresselhaus, *Carbon Nanotubes: Advanced Topics in the Synthesis, Structure, Properties and Applications*, Topics in Applied Physics Vol. 111 (Springer, Berlin, 2008).

[2] P. A. Williams, S. J. Papadakis, A. M. Patel, M. R. Falvo, S. Washburn, and R. Superfine, Phys. Rev. Lett. **89**, 255502 (2002).

[3] A. R. Hall, L. An, J. Liu, L. Vicci, M. R. Falvo, R. Superfine, and S. Washburn, Phys. Rev. Lett. **96**, 256102 (2006).

[4] E. Joselevich, ChemPhysChem **7**, 1405 (2006).

[5] A. Maiti, Nature Mater. **2**, 440 (2003).

[6] C. Gómez-Navarro, J. J. Sáenz, and J. Gómez-Herrero, Phys. Rev. Lett. **96**, 076803 (2006).

[7] T. Cohen-Karni, L. Segev, O. Srur-Lavi, S. R. Cohen, and E. Joselevich, Nat. Nanotechnol. **1**, 36 (2006).

[8] A. R. Hall, M. R. Falvo, R. Superfine, and S. Washburn, Nat.

Nanotechnol. **2**, 413 (2007).
[9] A. M. Fennimore, T. D. Yuzvinsky, W.-Q. Han, M. S. Fuhrer, J. Cumings, and A. Zettl, Nature (London) **424**, 408 (2003).
[10] S. J. Papadakis, A. R. Hall, P. A. Williams, L. Vicci, M. R. Falvo, R. Superfine, and S. Washburn, Phys. Rev. Lett. **93**, 146101 (2004).
[11] J. C. Meyer, M. Paillet, and S. Roth, Science **309**, 1539 (2005).
[12] L. Yang and J. Han, Phys. Rev. Lett. **85**, 154 (2000).
[13] B. Bourlon, C. Miko, L. Forró, D. C. Glattli, and A. Bachtold, Phys. Rev. Lett. **93**, 176806 (2004).
[14] F. Triozon, S. Roche, A. Rubio, and D. Mayou, Phys. Rev. B **69**, 121410(R) (2004).
[15] S. W. D. Bailey, D. Tománek, Y. K. Kwon, and C. J. Lambert, Europhys. Lett. **59**, 75 (2002).
[16] Y.-K. Kwon and D. Tománek, Phys. Rev. B **58**, R16001 (1998).
[17] S. Paulson, A. Hesler, M. B. Nardelli, R. M. Taylor, M. Falvo, R. Superfine, and S. Washburn, Science **290**, 1742 (2000).
[18] J.-C. Charlier, X. Blase, and S. Roche, Rev. Mod. Phys. **79**, 677 (2007).
[19] C. Nisoli, P. E. Lammert, E. Mockensturm, and V. H. Crespi, Phys. Rev. Lett. **99**, 045501 (2007).
[20] J. M. Soler, E. Artacho, J. D. Gale, A. García, J. Junquera, P. Ordejón, and D. Sánchez-Portal, J. Phys.: Condens. Matter **14**, 2745 (2002).
[21] B. T. Kelly, *Physics of Graphite* (Applied Science, London, 1981).